Organic Solar Cells with Graphene Electrodes and Vapor Printed Poly(3,4-ethylenedioxythiophene) as the Hole Transporting Layers
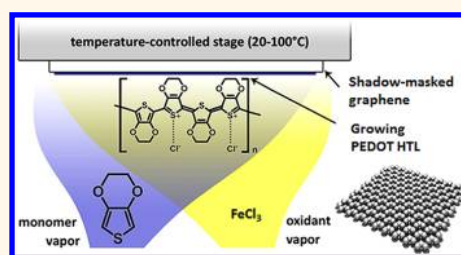
Hyesung Park,[†,§] Rachel M. Howden,[‡,§] Miles C. Barr,[‡] Vladimir Bulović,[†] Karen Gleason,[‡,*] and Jing Kong[†,*]

[†]Department of Electrical Engineering and Computer Science and [‡]Department of Chemical Engineering, Massachusetts Institute of Technology, Cambridge, Massachusetts 02139, United States. [§]These authors contributed equally to this work.

Graphene is the hexagonal arrangement of carbon atoms forming a one atom thick planar sheet. The successful isolation of single- and few-layer graphene by the mechanical cleaving of HOPG[1] has led to a significant increase in studies in numerous research areas. Of the many interesting properties of graphene (such as superior electron and hole mobility (up to 200 000 cm^2 V^{-1} s^{-1})[2,3] and high current carrying capability (up to 3 × 10^8 A cm^{-2})[4]), its uniformly high transparency in the visible and near-infrared region, with good electrical conductivity and mechanical robustness,[5] places graphene as a promising candidate for an alternative to indium tin oxide (ITO)[6] as a transparent conducting electrode (TCE).

Several criteria, such as electrical conductivity, optical transmittance, work function (WF), interfacial property with active layers, *etc.*, need to be considered for the integration of graphene sheets as TCEs in organic photovoltaics (OPV). Recent reports[7,8] have already demonstrated that graphene has high transmittance with moderate conductivity. However, generally lower WF of graphene as well as its interfacial properties with the adjacent active layer can be challenging in regard to the appropriate energy level alignment between the graphene and the highest occupied molecular orbital (HOMO) of the electron donor material. Bae *et al.*[8] reported a WF value of 4.27 eV for a monolayer of graphene synthesized from LPCVD, which is lower than for ITO (~4.5 eV and can be increased up to ~5.0 eV after oxygen (O$_2$) plasma treatment).[9,10] This low value for graphene is obviously not a good match for the electron donor material considered in this work (tetraphenyldibenzoperiflanthene (DBP), HOMO = 5.5 eV),[11] as well

as other common electron donor materials such as copper phthalocyanine (CuPc) (HOMO = 5.2 eV)[11] or poly(3-hexylthiophene) (P3HT) (HOMO = 5.2 eV),[12] which can induce a large energy barrier at the interface between the graphene and the organic layer.

For ITO anodes, a thin layer of conducting polymer, poly(3,4-ethylenedioxythiophene):poly(styrenesulfonate) (PEDOT:PSS), is

ABSTRACT

For the successful integration of graphene as a transparent conducting electrode in organic solar cells, proper energy level alignment at the interface between the graphene and the adjacent organic layer is critical. The role of a hole transporting layer (HTL) thus becomes more significant due to the generally lower work function of graphene compared to ITO. A commonly used HTL material with ITO anodes is poly(3,4-ethylenedioxythiophene) (PEDOT) with poly(styrenesulfonate) (PSS) as the solid-state dopant. However, graphene's hydrophobic surface renders uniform coverage of PEDOT:PSS (aqueous solution) by spin-casting very challenging. Here, we introduce a novel, yet simple, vapor printing method for creating patterned HTL PEDOT layers directly onto the graphene surface. Vapor printing represents the implementation of shadow masking in combination with oxidative chemical vapor deposition (oCVD). The oCVD method was developed for the formation of blanket (*i.e.*, unpatterned) layers of pure PEDOT (*i.e.*, no PSS) with systematically variable work function. In the unmasked regions, vapor printing produces complete, uniform, smooth layers of pure PEDOT over graphene. Graphene electrodes were synthesized under low-pressure chemical vapor deposition (LPCVD) using a copper catalyst. The use of another electron donor material, tetraphenyldibenzoperiflanthene, instead of copper phthalocyanine in the organic solar cells also improves the power conversion efficiency. With the vapor printed HTL, the devices using graphene electrodes yield comparable performances to the ITO reference devices ($\eta_{p,LPCVD}$ = 3.01%, and $\eta_{p,ITO}$ = 3.20%).

KEYWORDS: graphene · APCVD · LPCVD · organic solar cell · oCVD PEDOT · vapor printing · poly(3,4-ethylenedioxythiophene) · chemical vapor deposition

commonly inserted before the deposition of the electron donor material in order to favor an ohmic contact at the junction. The PEDOT:PSS hole transporting layer (HTL) with a WF of 5.2 eV not only facilitates the injection/extraction of holes but also is known to help planarize the rough surface of the ITO, which often becomes a possible source of local shorting through the ultrathin active layers, thus improving the overall device performance.[13,14] Therefore, smooth and complete coverage of the PEDOT:PSS layer on the underlying electrode surface plays a crucial role in the general OPV device performance. Application of PEDOT:PSS onto the graphene surface, on the other hand, has been challenging due to the fact that the graphene surface is hydrophobic but PEDOT:PSS is in an aqueous solution. The sputtered ITO surface is also hydrophobic, but it is almost always pretreated with O_2 plasma, which renders the hydrophobic surface into a hydrophilic one by introducing hydroxyl (OH) and carbonyl (C=O) groups[15] that enable conformal coverage of PEDOT:PSS. Active oxygen species from the plasma disrupt the aromatic rings of the graphene and greatly reduce the conductivity. In the case of single-layer graphene electrodes, a graphene film can completely lose the conductivity after such plasma treatments.

Recently, several groups have investigated the possible application of graphene-electrode-based OPV devices by addressing this interface issue. De Arco et al.[16] successfully demonstrated graphene-based flexible devices that are outperforming ITO control devices. Wang et al.[12] reported improved wetting of PEDOT:PSS on graphene via noncovalent chemical functionalization. Park et al.[17] also reported that the wettability of PEDOT:PSS on the graphene surface can be significantly improved by doping with gold(III) chloride ($AuCl_3$). However, the doping process introduces large Au particles (up to 100 nm in diameter), which can create shorting pathways through the device. Wang et al.[18] later reported using a molybdenum oxide (MoO_3) HTL with acid-doped graphene electrodes, which is a common HTL material used with ITO electrodes.[19] However, the device performance was not as efficient as the ITO control device with a MoO_3 layer alone and still required the use of PEDOT:PSS on top of the MoO_3 interfacial layer, which allowed better wetting of PEDOT:PSS on the MoO_3-coated graphene. On a slightly different note, Liu et al.[20] proposed the feasibility of solution-processable graphene as an acceptor material in polymer-based PV.

In this work, we introduce a novel, yet simple, HTL fabricated by vapor printing of PEDOT[21] directly onto the unmodified graphene surface. Previously, Wang et al.[22] reported similar work where they used the vapor-phase polymerized PEDOT as top anode for inverted solar cells. In a single step, vapor printing combines (i) the synthesis of conducting polymer chains from vapor-phase (3,4 ethylenedioxythiophene) (EDOT) monomer, (ii) thin film formation of the PEDOT HTL, and (iii) patterning by in situ shadow masking. Vapor printing is derived from the oxidative chemical vapor deposition (oCVD) (steps (i) and (ii) only). The oCVD blanket (i.e., unpatterned) PEDOT layers readily integrate with a wide range of substrates because it is a dry process and substrate temperature is mild (~120 °C), and the difficulties with film dewetting and substrate degradation by solvents or high temperatures can be completely avoided.[21] In addition, the WF of the oCVD PEDOT layer can be tuned by controlling the doping level of Cl^- ions.[23] In this work, we have found that the oCVD process is also compatible with graphene substrates. The oCVD polymer layer is formed by directly exposing the substrate to vaporized monomer EDOT and an oxidizing agent (in this case, $FeCl_3$) under controlled reactor conditions. The relatively mild deposition conditions (low temperature 120 °C, moderate pressure ~10 mTorr, and no use of solvents) allow for PEDOT to be deposited without damaging or delaminating the graphene electrode. Furthermore, as vapor printing is generally substrate independent, requiring no substrate-specific optimization of the oCVD process or substrate pretreatment, it allows the direct printing of the PEDOT onto our graphene substrates. The graphene-based solar cells fabricated with vapor printed PEDOT HTLs in this work achieve ~94% of the performance of their ITO counterparts without any additional treatment to the graphene sheets such as chemical doping.

RESULTS AND DISCUSSION

Graphene films were synthesized under low-pressure chemical vapor deposition (LPCVD) on Cu foils (25 μm in thickness and 99.8% purity, Alfa Aesar). This yields monolayer graphene on the Cu, and afterward, graphene anodes were prepared through layer-by-layer transfers by stacking three monolayers of graphene sheets. The average sheet resistance (R_{sh}) and transmittance values of the graphene electrodes are ~300 Ω/sq and ~92% (at 550 nm). Figure 1a illustrates the graphene synthesis and transfer process. After patterning the graphene electrodes, PEDOT (PEDOT:PSS or vapor printed PEDOT) and organic layers were subsequently deposited followed by the top capping electrode via thermal evaporation. The PEDOT deposition process is illustrated in Figure 1b. The final device structure was anode (ITO or graphene)/HTL (PEDOT:PSS or vapor printed PEDOT)/DBP/C_{60} (fullerene)/BCP (bathocuproine)/Al (aluminum). The complete solar cell structure is schematically shown in Figure 1c, and further details are explained in Methods.

Shown in Figure 2a are sheet resistance (R_{sh}) and transmittance values of vapor printed PEDOT with varying thicknesses. The thinner PEDOT layers (2, 7, and 15 nm) have higher transmittance values (generally
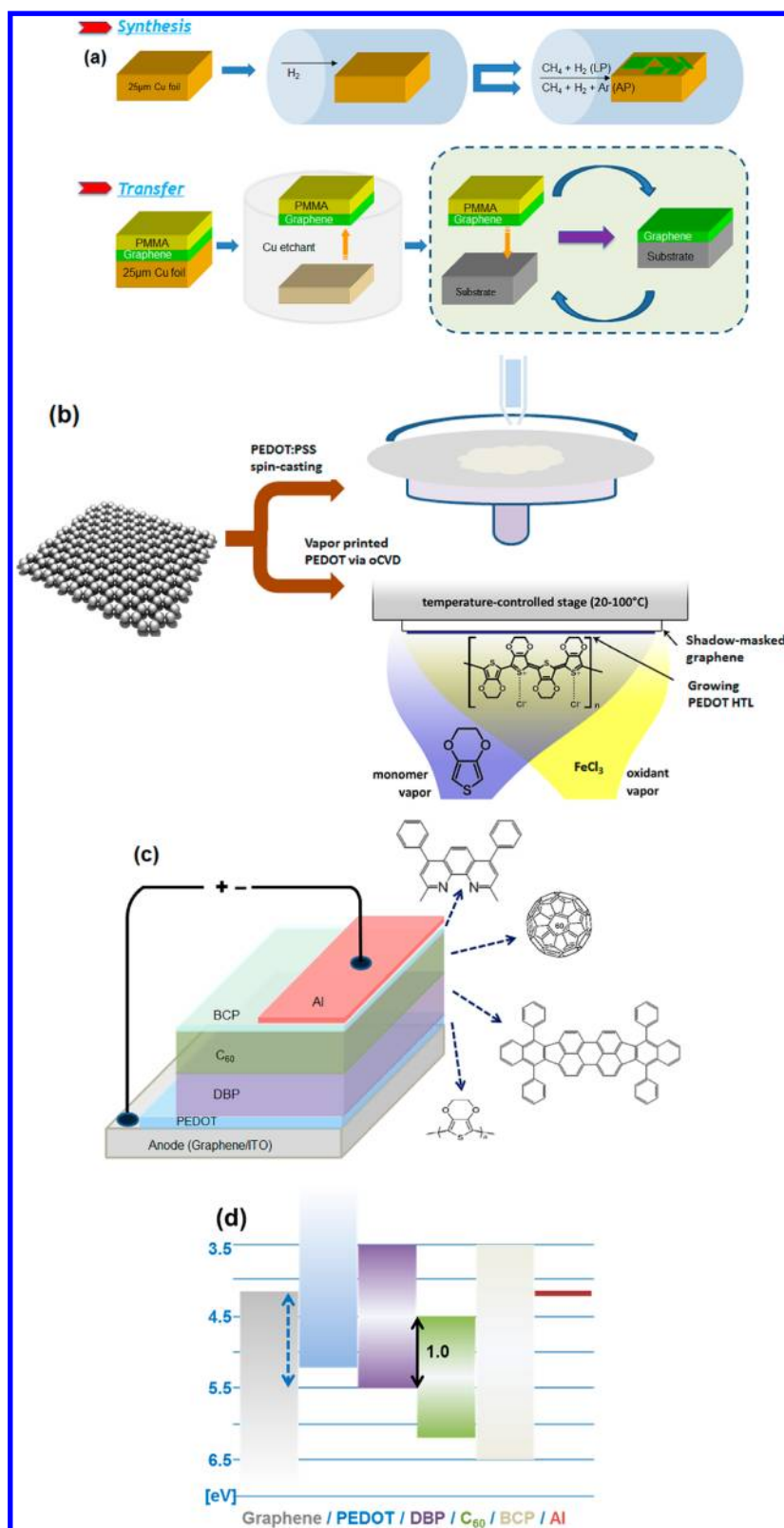
Figure 1. Schematics outlining the fabrication process of graphene electrodes, PEDOT HTLs, and OPV devices. (a) Graphene synthesis and transfer. The last part of the transfer procedure is repeated to prepare three-layer graphene stacks for LPCVD graphene. Detailed growth parameters are graphically illustrated in Supporting Information Figure S4. (b) PEDOT:PSS spin-coating *vs* vapor printing of PEDOT deposition. The spin-casting layer covers the graphene and the surrounding quartz substrate while the vapor printed patterns align to produce PEDOT only on the graphene electrodes. (c) Graphene/ITO anode OPV structure: Graphene(or ITO)/PEDOT/DBP/C$_{60}$/BCP/Al. (d) Flat-band energy level diagram of the complete OPV device structure.
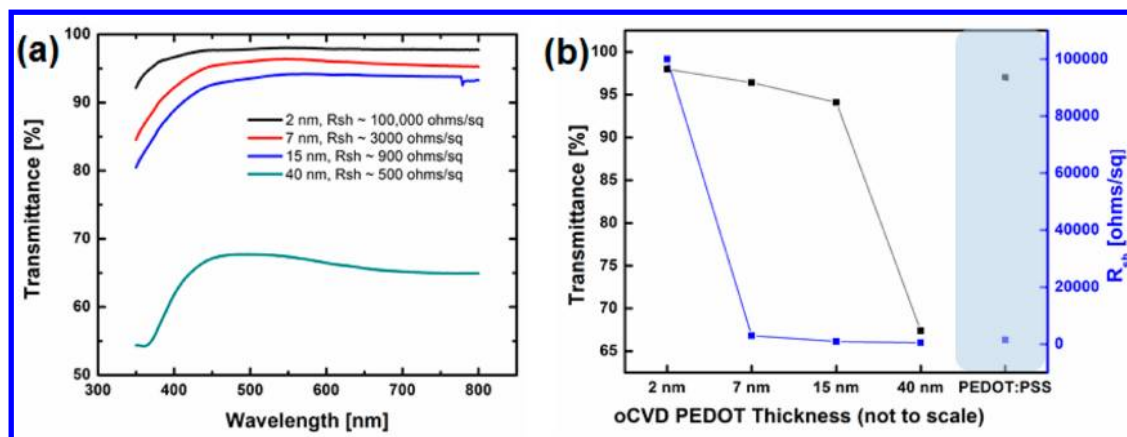
Figure 2. (a) Transmittance data for the oCVD PEDOT HTL layers, measured using ultraviolet−visible spectroscopy (UV−vis) over wavelengths from 350 to 800 nm. The oCVD PEDOT layers decrease in transmittance and sheet resistance with increasing thickness. The three thinnest PEDOT layers (2, 7, and 15 nm) have high transmittance values (>90% over a majority of the range), which are preferred for HTL layers. (b) Sheet resistance values for each thickness and the transmittance at 550 nm. The oCVD PEDOT sheet resistance was measured using a four-point probe (taking the average of 10 measurements). With increasing oCVD PEDOT thickness, there are more pathways for charge transfer, so the sheet resistance (R_{sh}) decreases. R_{sh} decreases dramatically from the thinnest (2 nm) to thicker PEDOT layers (7, 15, and 40 nm). Transmittance and R_{sh} values of PEDOT:PSS are also shown for comparison.

>90%) that are presumably better for HTL layers because losses in optical absorption through the transparent electrode could contribute to a decrease in device performance. On the other hand, the sheet resistance decreases with increasing thickness, with an abrupt change from 2 nm to the thicker layers (7, 15, and 40 nm) due to the amount of charge pathways increases (as shown in Figure 2b and Table S1). On the basis of the sheet resistance and thickness values of these films, the resistivity of the oCVD PEDOT can be derived, which are 20×10^{-3} $\Omega \cdot$cm (2 nm), 2.10×10^{-3} $\Omega \cdot$cm (7 nm), 1.35×10^{-3} $\Omega \cdot$cm (15 nm), and 2×10^{-3} $\Omega \cdot$cm (40 nm), respectively. It can be seen that the resistivity of the ≥ 7 nm films are consistent with each other because the same material is being deposited, but the resistivity of the 2 nm film is 1 order of magnitude higher, which is very likely that the film is not completely continuous at this level of thickness. Having a lower sheet resistance HTL results in better charge transfer to the graphene electrode; however, the thicker the HTL, the further the charge must travel through the layer to reach the graphene electrode and the greater the transmission losses due to absorption. Nevertheless, in our experiments, we have found that the thicknesses in the range of 7−40 nm all give reasonable performances.

Figure 3 shows the optical and SEM images of the graphene/quartz substrate after spin-coating PEDOT:PSS (left images, Figure 3a−c) in contrast with the vapor printed PEDOT (15 nm) (right images, Figure 3d−f). The optical image in Figure 3a shows that most of the spin-casted PEDOT:PSS dewets over the graphene electrode as well as the adjacent bare quartz (Figure 3b,c shows more details). The dewetting of the PEDOT:PSS is clearly observed over the entire substrate, which signifies that we do not have good

coverage of the graphene surface. In contrast, vapor printing provides a well-defined PEDOT region (light blue) (Figure 3d). Furthermore, the scanning electron microscopy (SEM) image in higher magnification shows that the coating of vapor printed PEDOT on graphene is uniform in finer detail (Figure 3f). Additional atomic force microscopy (AFM) images of oCVD PEDOT are shown in Figure S1. The oCVD PEDOT itself is relatively smooth, and conformal coverage on the graphene surface is confirmed by the reduced surface roughness of the pristine graphene. This confirms the understanding that, since oCVD is a dry process, the dewetting problem is avoided and the PEDOT can form a uniform film on the graphene.

Furthermore, the WF of vapor printed PEDOT on the graphene (three layers) was evaluated by the Kelvin probe method. The measured value averaged over several regions was ∼5.1 eV, which was similar to the commonly reported WF value of PEDOT:PSS (∼5.2 eV). This observation indicates that the injection/extraction of holes from the HOMO of the electron donor now becomes energetically favorable compared to the interface of graphene only.

Small molecule organic solar cells with graphene anodes were fabricated with device structures mentioned earlier. Figure 4a displays the current density−voltage ($J−V$) measurements of devices with various configurations using three-layer graphene anodes: graphene with spin-coated PEDOT:PSS and vapor printed PEDOT (15 nm) HTLs along with ITO reference. Due to the poor wetting of PEDOT:PSS, a graphene device with PEDOT:PSS typically shows the leaky behavior (not a diode behavior but rather like a linear resistor), and with poor photoresponse (much smaller V_{oc} and J_{sc}). On the other hand, the $J−V$ responses from the devices having vapor printed PEDOT HTLs (with different thicknesses
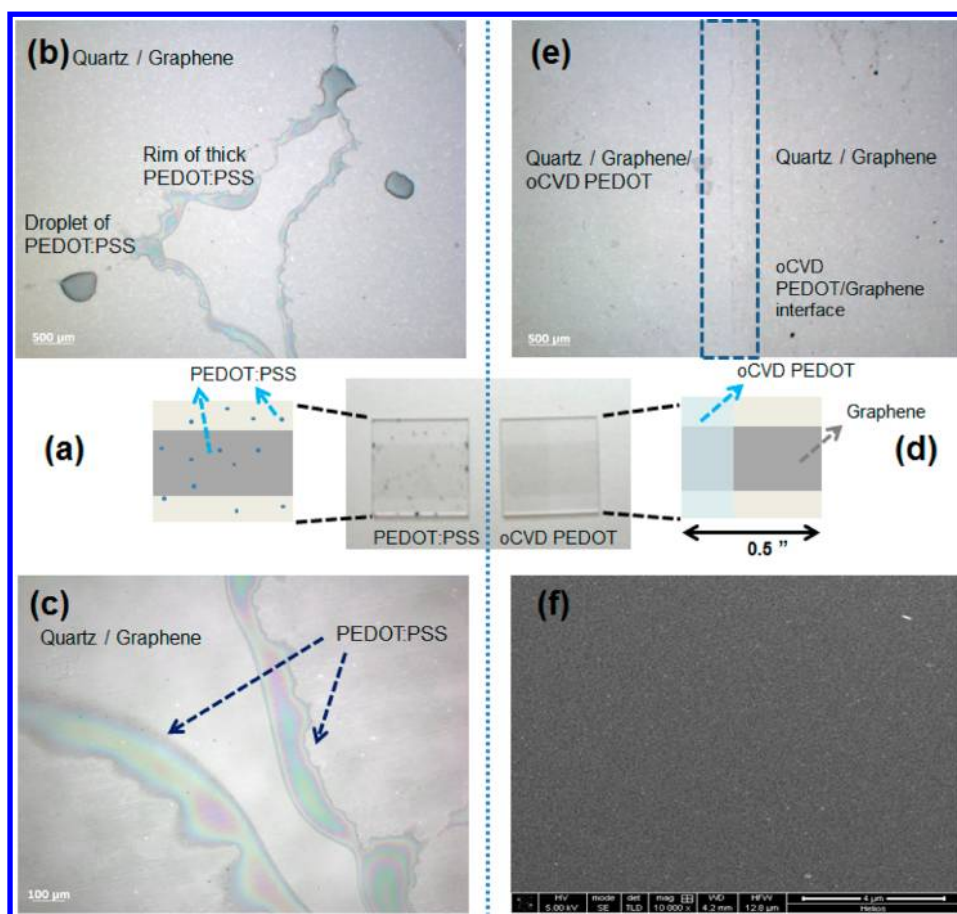
Figure 3. Comparing HTL coverage on quartz/graphene substrate. (a−c) Spin-coated PEDOT:PSS on quartz/graphene substrate, **(d−f)** oCVD PEDOT coating on quartz/graphene substrate. **(a)** Schematic illustration of PEDOT:PSS spin-coated on a quartz substrate with graphene electrode. Most of the PEDOT:PSS layer is dewetted from the substrate with dark macroscopic defects visible to the naked eye. **(b,c)** Optical micrographs (at different magnifications) of the spin-cast PEDOT: PSS on the graphene surface illustrating the poor wettability of PEDOT:PSS on the graphene. In contrast, **(d)** is the schematic illustration of CVD PEDOT coated *via* vapor deposition on quartz/graphene substrate, where a uniform coating and patterning *via* shadow masking is achieved. The left side in **(d)** has the oCVD PEDOT coating, whereas the right side is shadow masked. **(e)** Optical micrograph and **(f)** SEM image of oCVD PEDOT on graphene showing uniform coverage.

shown in Figure 4b,c for graphene and ITO electrodes) show good diode behavior and performance (J_{sc} (short-circuit current density) = 5.69 ± 0.17 mA cm^{-2}, V_{oc} (open-circuit voltage) = 0.88 ± 0.01 V, FF (fill factor) = 0.60 ± 0.01, and η_p (power conversion efficiency, PCE) = 3.01 ± 0.05%) is comparable to the ITO reference device with PEDOT:PSS (J_{sc} = 5.14 ± 0.12 mA cm^{-2}, V_{oc} = 0.92 ± 0.01 V, FF = 0.68 ± 0.01, and η_p = 3.20 ± 0.05%).

With more devices fabricated using the vapor printed PEDOT on graphene electrodes, we have found that about 30% among the working devices show the (close to) ideal diode *J−V* responses similar to the one presented in Figure 4a−c, and with the other working devices, nonideal behaviors have been observed (both for graphene and ITO electrodes), as shown in Figure S2a,b. Nevertheless, these nonideal performances are still considerably better than the performance obtained with devices having spin-coated PEDOT:PSS on graphene since, for the PEDOT:PSS HTL, the graphene-based devices almost never worked, as shown in Figure 4a. This ideal *versus* nonideal behavior does

not appear to be related to the thickness of the vapor printed PEDOT on graphene; as can be seen in both Figure 4b,c and Figure S2, for thicknesses between 7 and 40 nm, the devices have displayed both behaviors. Also, even within the devices that showed ideal behaviors, there appears to be no direct correlation between the PCE value and the PEDOT thickness. At present, the nonideal behavior appears to be a process-related issue and should be further investigated in the follow up work.

Apart from the successful interface engineering by the vapor printed oCVD PEDOT on graphene, another reason for the enhanced performance can be attributed to the increased V_{oc} observed in the cells compared to devices fabricated using CuPc as electron donor materials, one of the most widely used electron donor materials in the small-molecule-based OPV structure. As shown from the energy level diagram in Figure 1d, the maximum V_{oc} achievable from DBP/C$_{60}$ pair is ∼1.0 V, ∼0.3 V higher than CuPc/C$_{60}$. Therefore, improvements in V_{oc} mostly originate from the
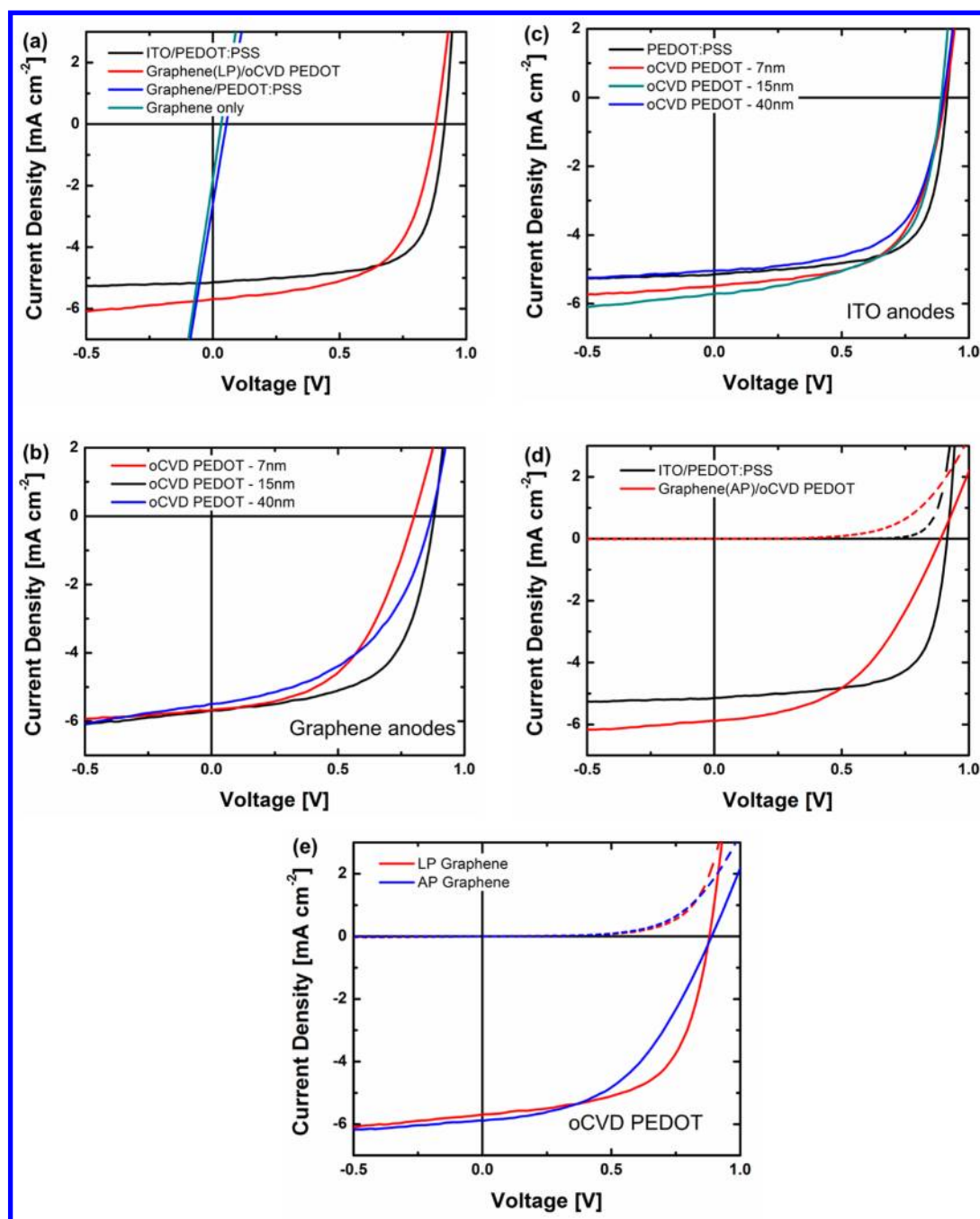
Figure 4. $J-V$ characteristics of representative graphene (three-layer, LPCVD)/ITO OPV devices (graphene, ITO/PEDOT:PSS (20 nm), vapor printed PEDOT (7–40 nm)/DBP, 25 nm/C_{60}, 40 nm/BCP, 7.5 nm/Al, 100 nm) under simulated AM 1.5G illumination at 100 mW/cm^2. (a) Graphene devices with PEDOT:PSS and vapor printed PEDOT (15 nm) HTL, compared with ITO/PEDOT:PSS reference device. (b) Graphene-anode-based cells with varying thicknesses of vapor printed PEDOT (7, 15, 40 nm). (c) ITO anode devices with varying vapor printed PEDOT thicknesses (7, 15, 40 nm) and a PEDOT:PSS reference. (d) $J-V$ characteristics of representative graphene (APCVD) OPV devices (graphene/vapor printed PEDOT, 15 nm/DBP, 25 nm/C_{60}, 40 nm/BCP, 7.5 nm/Al, 100 nm) along with ITO/PEDOT:PSS reference device under simulated AM 1.5G illumination at 100 mW/cm^2. (e) Comparison of graphene-based device performances, where graphene electrodes are prepared under either LPCVD or APCVD conditions.

deep-lying HOMO level of DBP compared to that of CuPc.

Graphene synthesized from the Cu catalyst under LP condition succeeded in producing high-quality monolayer sheets, which could not be achieved using nickel catalyst.[24,25] However, due to the self-limiting process

of the LPCVD, achieving multilayers of graphene from the Cu under LPCVD has been difficult.[24] In practice, a monolayer of graphene sheet can be hardly used as an electrode due to defects induced from processing issues, such as transfer or patterning, as well as the generally lower conductivity compared to stacked

multilayers (R_{sh} decreases as a function of additional layers[17]). On the other hand, transferring multiple steps to obtain multilayers adds complexity and cost to the fabrication process. Therefore, in this work, we also carried out few-layer graphene synthesis under atmospheric CVD (APCVD) condition using Cu foils, where only one-step transfer is needed for graphene electrodes. Figure S3a,c shows the optical and AFM images of the APCVD-grown graphene, which has a non-uniform film thickness, and the optical and AFM images of LPCVD graphene are also presented in Figure S3b,d for comparison. The APCVD graphene layers have average sheet resistance and transmittance values of ~450 Ω/sq and ~92% (at 550 nm), respectively. Even though the thicknesses of the APCVD-grown graphene layers are non-uniform, we have verified that the vapor printing of oCVD PEDOT onto these graphene layers is as successful as the LPCVD graphene layers. This is consistent with the general observation that oCVD PEDOT deposition is substrate independent and it coats uniformly on the substrate.

Solar cells fabricated with graphene anodes prepared under APCVD conditions demonstrated reasonable performances, although the efficiency was slightly less than devices made via LPCVD conditions ($\eta_{p,APCVD}$ = 2.49% and $\eta_{p,LPCVD}$ = 3.01%). Figure 4d shows the $J-V$ characteristics of a graphene device with vapor printed PEDOT (J_{sc} = 5.89 ± 0.03 mA cm^{-2}, V_{oc} = 0.89 ± 0.03 V, FF = 0.48 ± 0.01, and η_p = 2.49 ± 0.06%) and ITO reference device with PEDOT:PSS (J_{sc} = 5.14 ± 0.12 mA cm^{-2}, V_{oc} = 0.92 ± 0.01 V, FF = 0.68 ± 0.01, and η_p = 3.20 ± 0.05%). Figure 4e compares the best device performance using graphene electrodes from different synthesis conditions (LPCVD vs APCVD), where APCVD graphene device performs ~83% of LPCVD graphene-based device. At the moment, the performance of APCVD graphene-based devices is limited to the generally higher sheet resistance than LPCVD graphene. We are currently investigating to improve the quality of the graphene electrodes fabricated under APCVD condition to achieve comparable device performances to LPCVD-based counterparts.

CONCLUSION

In summary, we introduce a novel, yet simple, method for vapor printing PEDOT onto the graphene surface, which yields well-defined patterns using in situ shadow masking. The oCVD process, which is the foundation for vapor printing, results in smooth, complete coverage of PEDOT on the graphene electrode. In contrast, spin-casting PEDOT:PSS from an aqueous solution does not coat the graphene surface, as well, due to graphene's low surface free energy.[26] The oCVD process works well on both LPCVD-grown graphene (with uniform thicknesses) and APCVD-grown graphene (with non-uniform thicknesses). Furthermore, the use of small molecular electron donor material DBP combined with the vapor printed PEDOT HTL yields more efficient graphene-based devices with performances comparable to those of ITO reference devices. The results here represent a further step forward in the investigation of using graphene as an alternative TCE for the replacement of ITO and open up opportunities in other applications, as well, such as organic light-emitting diodes (OLEDs).

METHODS

Graphene Synthesis (LPCVD, APCVD). Copper foil (25 μm in thickness, Alfa Aesar) was used as a metal catalyst for both conditions. LPCVD. The CVD chamber was evacuated to a base pressure of 30–50 mTorr. The system was then heated to a growth temperature of 1000 °C under hydrogen (H$_2$, 10 sccm) gas (~320 mTorr) and annealed for 30 min. Subsequently, methane (CH$_4$, 20 sccm) gas was introduced (total pressure ~810 mTorr), and graphene growth was carried out for 30 min. The chamber was then cooled at ~45 °C/min to room temperature. APCVD. The chamber was heated to 1000 °C under H$_2$ gas (170 sccm) and annealed for 30 min. After annealing, H$_2$ was reduced to 30 sccm and CH$_4$ (1 sccm) and Ar (1000 sccm) were additionally introduced followed by 30 min of growth. After growth, the chamber was cooled at ~100 °C/min to room temperature. Both processes are schematically illustrated in Supporting Information Figure S3.

Graphene Transfer and Anode Preparation. Transfer was carried out using poly(methyl methacrylate) (PMMA, 950 A9, Microchem). Graphene on one side of the foil was removed via reactive ion etching (RIE) with O$_2$ gas (Plasma-Therm, 100 W at 7 × 10^{-5} Torr). Cu was etched by a commercial etchant (CE-100, Transene). Graphene films were then thoroughly rinsed with diluted hydrochloric acid (10%) and deionized (DI) water to remove residual iron ions from the Cu etchant. The PMMA layer was removed by annealing at 500 °C for 2 h under H$_2$ (700 sccm) and Ar (400 sccm). Repeated transfers were performed for three-layer graphene films. The transferred graphene films were patterned into the desired shape through RIE.

Vapor Deposition Polymerized PEDOT. The oCVD reactor configuration and general process procedure are described elsewhere.[27] The oCVD PEDOT HTLs were all deposited under the same reaction conditions. The reactor pressure was held at ~10 mTorr, and the substrate temperature was maintained at 120 °C. The monomer 3,4-ethylenedioxythiophene (Sigma Aldrich, 97%), EDOT, was used as purchased. The EDOT was heated to 140 °C and introduced into the reactor at a flow rate of ~5 sccm. Iron(III) chloride (Sigma Aldrich, 99.99%) was evaporated from a heated crucible between 130 and 160 °C. Different thicknesses were achieved by varying the time of reaction (1, 2, 4, and 8 min, respectively, to get HTL thicknesses of 2, 7, 15, and 40 nm). PEDOT:PSS (Clevios P VP AI 4083) was filtered (0.45 μm), spin-coated at 4000 rpm for 60 s, and annealed at 210 °C for 5 min in air. The PEDOT was patterned using a precut metal shadow mask with the same dimensions as the graphene electrode. The mask was visually aligned such that the PEDOT was deposited directly on top of the graphene.

OPV Device Fabrication Process. Organic layers (DBP (Luminescence Technology Corp., >99%), C$_{60}$ (Sigma Aldrich, 99.9%), BCP (Luminescence Technology Corp., >99%)), and top cathode (Al (Alfa Aesar, 3.175 mm slug, 99.999%)) were thermally evaporated through shadow masks at a base pressure of 1 × 10^{-6} Torr at rates of 1.0 and 1.5 Å/s, respectively. C$_{60}$ was purified once via thermal gradient sublimation before use.

DBP, BCP, and Al were used as received. Prepatterned ITO (thin film devices, 20 Ω/sq) substrates were cleaned by solvents followed by 30 s of O_2 plasma (100 W, Plasma Preen, Inc.). Patterned graphene substrates were cleaned by annealing at 500 °C for 30 min under H_2 (700 sccm) and Ar (400 sccm). The device area defined by the opening of the shadow mask was 1.21 mm^2.

Measurements. The surface morphology of the graphene sheet was characterized by AFM (Dimension 3100, Veeco), and the transmittance was measured from the UV−vis−NIR spectrometer (Cary 5000, Varian). Work function measurements were performed using a SKP5050 Kelvin probe system from Kelvin Technology Inc. with analysis taken at various locations on each sample with 50 measurements collected per location (using 30 point averaging). Current−voltage measurements were recorded by a Keithley 6487 picoammeter in nitrogen atmosphere, and 100 mW cm^{-2} illumination was provided by 150 W xenon arc-lamp (Newport 96000) filtered by an AM 1.5G filter.

Conflict of Interest: The authors declare no competing financial interest.

Supporting Information Available: Additional information on AFM images of oCVD PEDOT, current density−voltage curves of graphene/ITO anodes with varying vapor printed PEDOT thicknesses, optical/AFM images of APCVD/LPCVD graphene films with corresponding growth parameters. This material is available free of charge *via* the Internet at http://pubs.acs.org.

REFERENCES AND NOTES

1. Novoselov, K. S.; Jiang, D.; Schedin, F.; Booth, T. J.; Khotkevich, V. V.; Morozov, S. V.; Geim, A. K. Two-Dimensional Atomic Crystals. *Proc. Natl. Acad. Sci. U.S.A.* **2005**, *102*, 10451−10453.
2. Berger, C.; Song, Z. M.; Li, X. B.; Wu, X. S.; Brown, N.; Naud, C.; Mayou, D.; Li, T. B.; Hass, J.; Marchenkov, A. N.; *et al.* Electronic Confinement and Coherence in Patterned Epitaxial Graphene. *Science* **2006**, *312*, 1191−1196.
3. Bolotin, K. I.; Sikes, K. J.; Jiang, Z.; Klima, M.; Fudenberg, G.; Hone, J.; Kim, P.; Stormer, H. L. Ultrahigh Electron Mobility in Suspended Graphene. *Solid State Commun.* **2008**, *146*, 351−355.
4. Moser, J.; Barreiro, A.; Bachtold, A. Current-Induced Cleaning of Graphene. *Appl. Phys. Lett.* **2007**, *91*, 163513.
5. Bunch, J. S.; van der Zande, A. M.; Verbridge, S. S.; Frank, I. W.; Tanenbaum, D. M.; Parpia, J. M.; Craighead, H. G.; McEuen, P. L. Electromechanical Resonators from Graphene Sheets. *Science* **2007**, *315*, 490−493.
6. Eda, G.; Fanchini, G.; Chhowalla, M. Large-Area Ultrathin Films of Reduced Graphene Oxide as a Transparent and Flexible Electronic Material. *Nat. Nanotechnol.* **2008**, *3*, 270−274.
7. Kim, K. K.; Reina, A.; Shi, Y. M.; Park, H.; Li, L. J.; Lee, Y. H.; Kong, J. Enhancing the Conductivity of Transparent Graphene Films *via* Doping. *Nanotechnology* **2010**, *21*, 285205.
8. Bae, S.; Kim, H.; Lee, Y.; Xu, X. F.; Park, J. S.; Zheng, Y.; Balakrishnan, J.; Lei, T.; Kim, H. R.; Song, Y. I.; *et al.* Roll-to-Roll Production of 30-Inch Graphene Films for Transparent Electrodes. *Nat. Nanotechnol.* **2010**, *5*, 574−578.
9. Park, Y.; Choong, V.; Gao, Y.; Hsieh, B. R.; Tang, C. W. Work Function of Indium Tin Oxide Transparent Conductor Measured by Photoelectron Spectroscopy. *Appl. Phys. Lett.* **1996**, *68*, 2699−2701.
10. Milliron, D. J.; Hill, I. G.; Shen, C.; Kahn, A.; Schwartz, J. Surface Oxidation Activates Indium Tin Oxide for Hole Injection. *J. Appl. Phys.* **2000**, *87*, 572−576.
11. Fujishima, D.; Kanno, H.; Kinoshita, T.; Maruyama, E.; Tanaka, M.; Shirakawa, M.; Shibata, K. Organic Thin-Film Solar Cell Employing a Novel Electron-Donor Material. *Sol. Energy Mater. Sol. Cells* **2009**, *93*, 1029−1032.
12. Wang, Y.; Chen, X. H.; Zhong, Y. L.; Zhu, F. R.; Loh, K. P. Large Area, Continuous, Few-Layered Graphene as Anodes in Organic Photovoltaic Devices. *Appl. Phys. Lett.* **2009**, *95*, 063302.
13. Gunes, S.; Neugebauer, H.; Sariciftci, N. S. Conjugated Polymer-Based Organic Solar Cells. *Chem. Rev.* **2007**, *107*, 1324−1338.
14. Peumans, P.; Forrest, S. R. Very-High-Efficiency Double-Heterostructure Copper Phthalocyanine/C_{60} Photovoltaic Cells. *Appl. Phys. Lett.* **2001**, *79*, 126−128.
15. Murakami, T. N.; Fukushima, Y.; Hirano, Y.; Tokuoka, Y.; Takahashi, M.; Kawashima, N. Surface Modification of Polystyrene and Poly(methyl methacrylate) by Active Oxygen Treatment. *Colloids Surf., B* **2003**, *29*, 171−179.
16. De Arco, L. G.; Zhang, Y.; Schlenker, C. W.; Ryu, K.; Thompson, M. E.; Zhou, C. W. Continuous, Highly Flexible, and Transparent Graphene Films by Chemical Vapor Deposition for Organic Photovoltaics. *ACS Nano* **2010**, *4*, 2865−2873.
17. Park, H.; Rowehl, J. A.; Kim, K. K.; Bulovic, V.; Kong, J. Doped Graphene Electrodes for Organic Solar Cells. *Nanotechnology* **2010**, *21*, 6.
18. Wang, Y. W. Y.; Tong, S. W.; Xu, X. F.; Ozyilmaz, B.; Loh, K. P. Interface Engineering of Layer-by-Layer Stacked Graphene Anodes for High-Performance Organic Solar Cells. *Adv. Mater.* **2011**, *23*, 1514−1518.
19. Cattin, L.; Dahou, F.; Lare, Y.; Morsli, M.; Tricot, R.; Houari, S.; Mokrani, A.; Jondo, K.; Khelil, A.; Napo, K.; *et al.* MoO_3 Surface Passivation of the Transparent Anode in Organic Solar Cells Using Ultrathin Films. *J. Appl. Phys.* **2009**, *105*, 034507.
20. Liu, Q.; Liu, Z. F.; Zhong, X. Y.; Yang, L. Y.; Zhang, N.; Pan, G. L.; Yin, S. G.; Chen, Y.; Wei, J. Polymer Photovoltaic Cells Based on Solution-Processable Graphene and P3HT. *Adv. Funct. Mater.* **2009**, *19*, 894−904.
21. Barr, M. C.; Rowehl, J. A.; Lunt, R. R.; Xu, J.; Wang, A.; Boyce, C. M.; Im, S. G.; Bulović, V.; Gleason, K. K. Direct Monolithic Integration of Organic Photovoltaic Circuits on Unmodified Paper. *Adv. Mater.* **2011**, *23*, 3500−3505.
22. Wang, X. J.; Ishwara, T.; Gong, W.; Campoy-Quiles, M.; Nelson, J.; Bradley, D. D. C. High-Performance Metal-Free Solar Cells Using Stamp Transfer Printed Vapor Phase Polymerized Poly(3,4-ethylenedioxythiophene) Top Anodes. *Adv. Funct. Mater.* **2012**, *22*, 1454−1460.
23. Im, S. G.; Gleason, K. K.; Olivetti, E. A. Doping Level and Work Function Control in Oxidative Chemical Vapor Deposited Poly(3,4-ethylenedioxythiophene). *Appl. Phys. Lett.* **2007**, *90*, 152112.
24. Li, X. S.; Cai, W. W.; An, J. H.; Kim, S.; Nah, J.; Yang, D. X.; Piner, R.; Velamakanni, A.; Jung, I.; Tutuc, E.; *et al.* Large-Area Synthesis of High-Quality and Uniform Graphene Films on Copper Foils. *Science* **2009**, *324*, 1312−1314.
25. Reina, A.; Jia, X. T.; Ho, J.; Nezich, D.; Son, H. B.; Bulovic, V.; Dresselhaus, M. S.; Kong, J. Large Area, Few-Layer Graphene Films on Arbitrary Substrates by Chemical Vapor Deposition. *Nano Lett.* **2009**, *9*, 30−35.
26. Wang, S. R.; Zhang, Y.; Abidi, N.; Cabrales, L. Wettability and Surface Free Energy of Graphene Films. *Langmuir* **2009**, *25*, 11078−11081.
27. Lock, J. P.; Im, S. G.; Gleason, K. K. Oxidative Chemical Vapor Deposition of Electrically Conducting Poly(3,4-ethylenedioxythiophene) Films. *Macromolecules* **2006**, *39*, 5326−5329.